

# Seismic response of fractures and induced anisotropy in poroelastic media

Rock Physics Workshop, Quindao, October 25-27,  
201

**Juan E. Santos,**

Instituto del Gas y del Petróleo (IGPUBA), Universidad de Buenos Aires (UBA), Argentina, Department of Mathematics, Purdue University, West Lafayette, Indiana, USA,

October 16, 2019

# Seismic waves in fractured fluid-saturated poroelastic materials.

- A planar fracture embedded in a fluid-saturated poroelastic – Biot - medium can be modeled as a extremely thin, highly permeable and compliant porous layer.
- A Biot medium containing a dense set of aligned fractures behaves as an effective **transversely isotropic and viscoelastic medium (TIV)** when the average fracture distance is much smaller than the predominant wavelength of the traveling waves.
- This leads to frequency and angular variations of velocity and attenuation of seismic waves.

# Seismic waves in fractured fluid-saturated poroelastic materials.



- P-waves traveling in this type of medium induce fluid-pressure gradients at fractures and mesoscopic-scale heterogeneities, generating fluid flow and slow (diffusion) Biot waves, causing attenuation and dispersion of the fast modes (**mesoscopic loss**).
- A poroelastic medium with embedded aligned fractures exhibits significant attenuation and dispersion effects due to this mechanism.
- Due to the **extremely fine meshes** needed to properly represent these mesoscopic-scale fractures, numerical simulations are very expensive or even not feasible.

# Seismic waves in fractured fluid-saturated poroelastic materials.



- **Our approach:** In the context of Numerical Rock Physics, we use a **numerical upscaling procedure** to determine the complex and frequency dependent stiffness at the macroscale of a **TIV** medium equivalent to a Biot medium with aligned fractures.
- To determine the complex stiffness coefficients of the **equivalent TIV medium at the macroscale**, we solve a set of boundary value problems (BVP's) for Biot's equation in the diffusive range.
- The BVP's are stated and solved in the space-frequency-domain using the finite-element method (**FEM**).

# Seismic waves in fractured fluid-saturated poroelastic materials.

IV

- The BVP's represent **harmonic tests** at a finite number of frequencies on a representative sample of the material.
- **Numerical Rock Physics** offer an alternative to laboratory measurements.
- Numerical experiments are inexpensive and informative since the physical process of wave propagation can be inspected during the experiment.
- Moreover, they are **repeatable, essentially free from experimental errors**, and may easily be run using alternative models of the rock and fluid properties.

- For Biot's media, White et al. (1975) were the first to introduce the mesoscopic-loss mechanism in the framework of Biot's theory.
- For fine layered poroelastic materials, the theories of Gelinsky and Shapiro (GPY, 62, 1997) and Krzikalla and Müller (GPY, 76, 2011) allow to obtain the **five** complex and frequency-dependent stiffnesses of the **equivalent TIV medium**.
- To provide a more general modeling tool, we present a **numerical upscaling procedure** to obtain the complex stiffnesses of the effective **TIV** medium.

- We employ the FEM to solve in the space-frequency domain **Biot's equations in the diffusive range** with boundary conditions representing **compressibility and shear harmonic** experiments.
- The methodology is applied to saturated isotropic poroelastic samples having a dense set of horizontal fractures.
- The samples contained mesoscopic-scale heterogeneities due to patchy brine-CO<sub>2</sub> saturation and fractal porosity and consequently, fractal permeability and frame properties.

Consider isotropic fluid-saturated poroelastic layers.  
 $\mathbf{u}^s(\mathbf{x}), \mathbf{u}^f(\mathbf{x})$  : time Fourier transform of the  
 displacement vector of the solid and fluid relative to the  
 solid frame, respectively.

$$\mathbf{u} = (\mathbf{u}^s, \mathbf{u}^f)$$

$\sigma_{kl}(u), \mathbf{p}_f(u)$ : Fourier transform of the total stress and  
 the fluid pressure, respectively

On each plane layer  $n$  in a sequence of  $N$  layers, the  
**frequency-domain stress-strain relations** are

$$\begin{aligned}\sigma_{kl}(u) &= 2\mu \varepsilon_{kl}(u^s) + \delta_{kl} \left( \lambda_G \nabla \cdot u^s + \alpha M \nabla \cdot u^f \right), \\ \mathbf{p}_f(u) &= -\alpha M \nabla \cdot u^s - M \nabla \cdot u^f.\end{aligned}$$

## Biot's equations in the diffusive range:

$$\begin{aligned}\nabla \cdot \sigma(u) &= 0, \\ i\omega \frac{\eta}{\kappa} u^f(x, \omega) + \nabla p_f(u) &= 0,\end{aligned}$$

$\omega = 2\pi f$ : **angular frequency**

$\eta$ : **fluid viscosity**       $\kappa$ : **frame permeability**

$\tau_{ij}$ : stress tensor of the equivalent TIV medium  
 For a closed system ( $\nabla \cdot u^f = 0$ ), the corresponding  
**stress-strain relations**, stated in the space-frequency  
 domain, are

$$\tau_{11}(u) = p_{11} \epsilon_{11}(u^s) + p_{12} \epsilon_{22}(u^s) + p_{13} \epsilon_{33}(u^s),$$

$$\tau_{22}(u) = p_{12} \epsilon_{11}(u^s) + p_{11} \epsilon_{22}(u^s) + p_{13} \epsilon_{33}(u^s),$$

$$\tau_{33}(u) = p_{13} \epsilon_{11}(u^s) + p_{13} \epsilon_{22}(u^s) + p_{33} \epsilon_{33}(u^s),$$

$$\tau_{23}(u) = 2 p_{55} \epsilon_{23}(u^s),$$

$$\tau_{13}(u) = 2 p_{55} \epsilon_{13}(u^s),$$

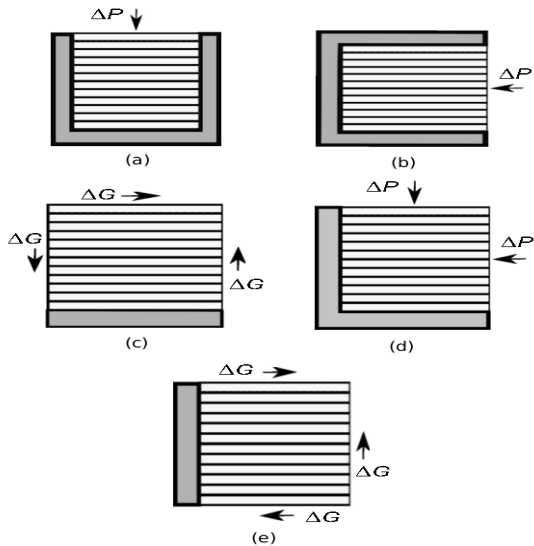
$$\tau_{12}(u) = 2 p_{66} \epsilon_{12}(u^s).$$

This approach provides the complex velocities of the  
 fast modes and takes into account **interlayer flow  
 effects**.

# A TIV medium equivalent to a Biot's medium with aligned fractures. III

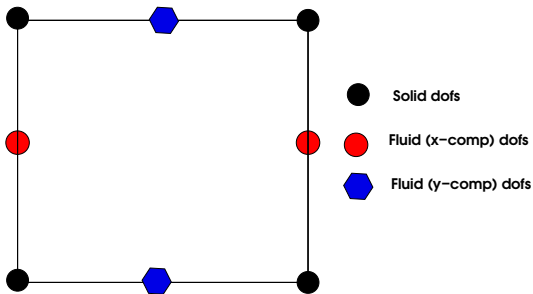
- In the context of **Numerical Rock Physics** the complex stiffness coefficients  $p_{IJ}(\omega)$  are determined using five time-harmonic experiments, each one associated with a BVP.
- The BVP's consist on **compressibility and shear tests** on a sample of Biot material with a dense set of fractures modeled using **B. C.**
- The BVP's are formulated in the space-frequency domain and solved using th FEM.
- This approach offers an alternative to laboratory measurements. It is essentially free from experimental errors and can easily be run using alternative models of the materials being analyzed.

## The experiments to determine the five $p_{IJ}$ TIV stiffness



(l) : Figs (a) and (b) show how to determine  $p_{33}$  and  $p_{11}$ , (c) determines  $p_{55}$ , (e) determines  $p_{66}$  and (d) determines  $p_{13}$ .

# Local degrees of freedom for the FEM solution of the harmonic tests.



The solution of the oscillatory tests was computed using the **FEM**. The figure displays the local degrees of freedom (**DOFs**) associated with each component of the solid displacement and the fluid displacement vectors.

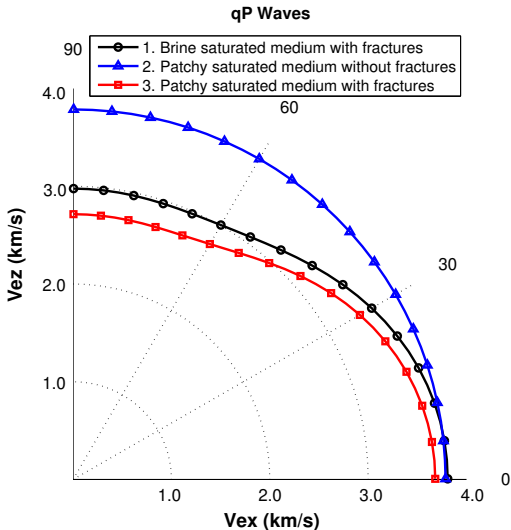
Consider the following cases for a square poroelastic sample of 160 cm side length and 10 periods of 1 cm fracture, 15 cm background:

- Case 1: A brine-saturated sample with fractures.
- Case 2: A brine-CO<sub>2</sub> patchy saturated sample without fractures.
- Case 3: A brine-CO<sub>2</sub> patchy saturated sample with fractures.
- Case 4: A brine saturated sample with a fractal frame and fractures.

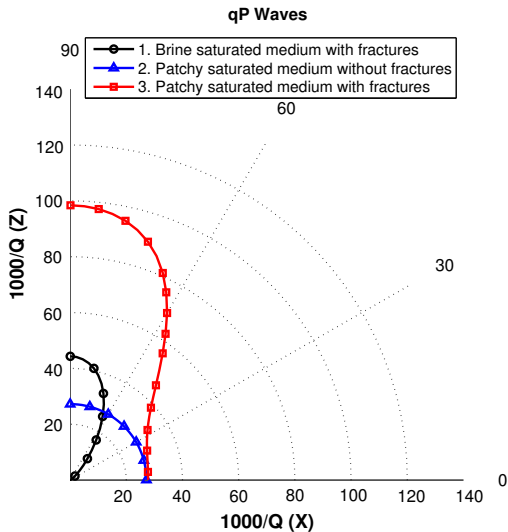
The complex stiffnesses  $p_{IJ}(\omega)$  were determined for 30 frequencies using a public domain sparse matrix solver.

The  $p_{IJ}(\omega)$ 's determine the energy velocities and dissipation coefficients shown in the next figures.

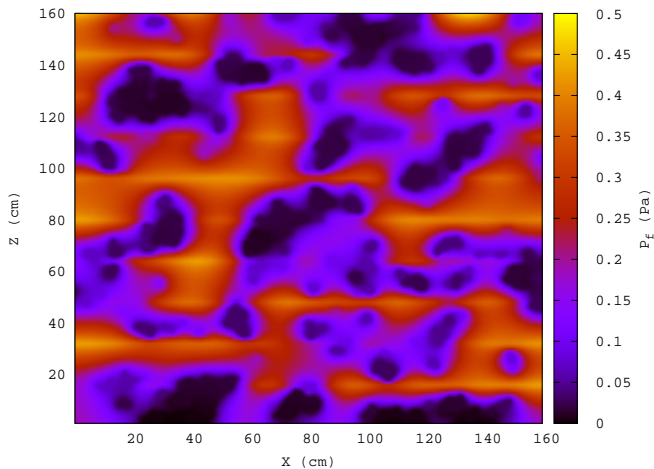
Polar representation of energy velocity vector of qP waves at 50 Hz for Cases 1, 2 and 3



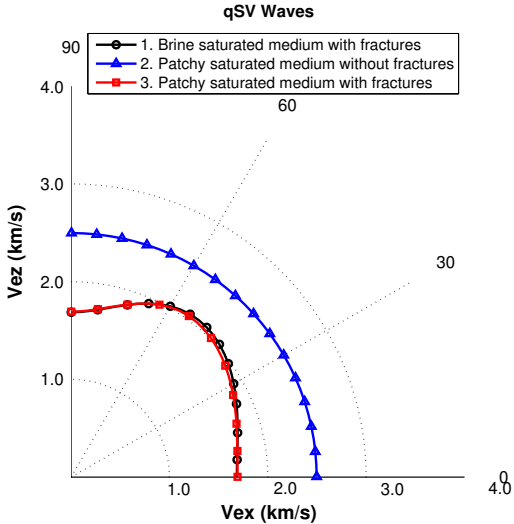
Cases 1 and 3 show velocity anisotropy caused by fractures. Case 3 (patchy saturation) exhibits lower velocities. Velocity behaves isotropically in Case 2.



Fractures induce strong Q anisotropy for angles normal to the fracture plane, enhanced by patchy saturation.

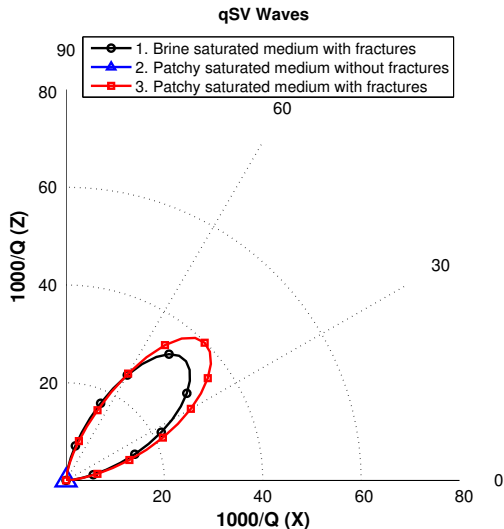


Compression is normal to the fracture plane.



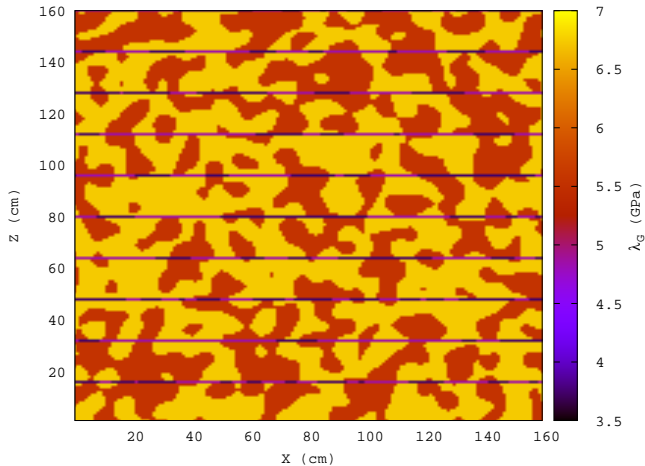
Velocity anisotropy is induced by fractures (Cases 1 and 3 ). Patchy saturation does not affect the anisotropic behavior of qSV velocities. Case 2 is isotropic with higher velocity values than for the fractured cases.

Polar representation of dissipation factor of qSV waves at 50 Hz for Cases 1, 2 and 3

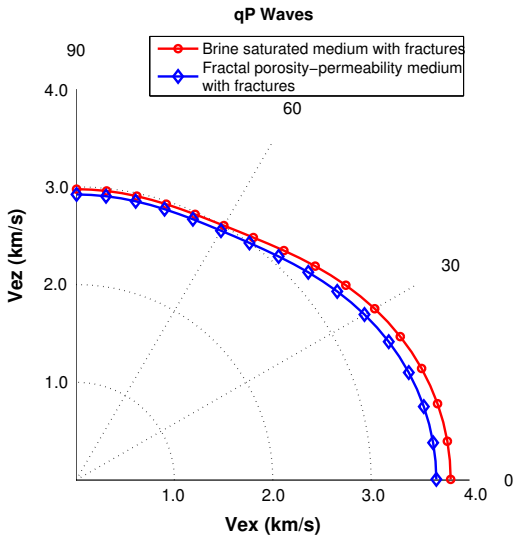


qSV attenuation anisotropy is strong for angles between 30 and 60 degrees. The lossless Case 2 is represented by a triangle at the origin.

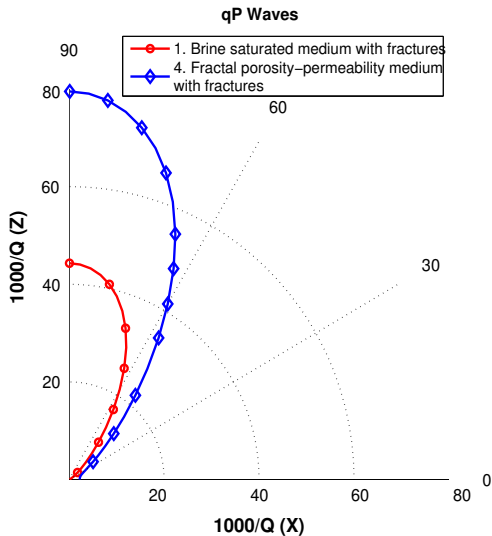
Lamé coefficient (GPa) for the brine-saturated fractal porosity-permeability sample of case 4.



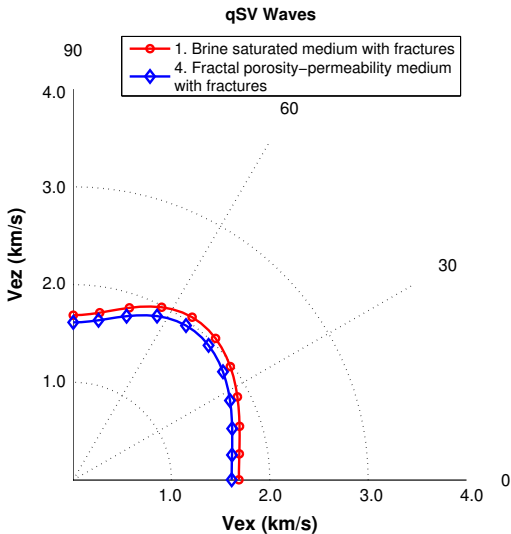
$\log \kappa(x, z) = \langle \log \kappa \rangle + f(x, z)$ ,  $f(x, z)$ : fractal representing the spatial fluctuation of the permeability field  $\kappa(x, z)$ .



Note the decrease in qP energy velocity for angles normal to the fracture plane.

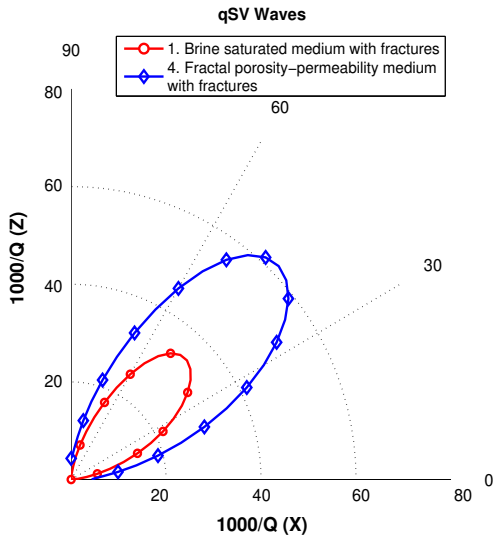


Note the increase in Q anisotropy for qP waves for angles normal to the fracture plane.



There is decrease in qSV velocity for Case 4

Polar representation of dissipation factor of qSV waves at 50 Hz for cases 1 and 4.



Attenuation of qSV waves is strong for angles between 30 and 60 degrees, and higher in Case 4.

We solve the following boundary value problem at the macroscale in a domain  $\Omega$  with boundary  $\partial\Omega$ :

$$\begin{aligned}\omega^2 \rho u + \nabla \cdot \tau(u) &= F, & \Omega \\ -\tau(u)\nu &= i\omega \mathcal{D}u, & \partial\Omega, (\text{absorbing B. C.}, D > 0)\end{aligned}$$

$u = (u_x, u_z)$ : macroscopic displacement vector,  $\rho$ : average density.

$\tau(u)$ : stress-tensor of our **equivalent TIV medium**, defined in terms of the  $p'_{IJ}$ s.

A global continuous variational formulation: Find  $u(x, \omega) \in [H^1(\Omega)]^2$  such that

$$-(\rho\omega^2 u, \varphi) + (\tau(u), \varepsilon(\varphi)) + i\omega \langle \mathcal{D}u, \varphi \rangle_{\partial\Omega} = (f, \varphi), \quad \varphi \in [H^1$$